Available online at www.sciencedirect.com
ScienceDirect
International Journal of Heat and Mass Transfer 50 (2007) 1442–1454
International Journal of HEAT and MASS TRANSFER
www.elsevier.com/locate/ijhmt

Saturated flow boiling heat transfer of refrigerant R-410A in a horizontal annular finned duct

Y.Y. Hsieh [a], Y.M. Lie [b], T.F. Lin [b,*]

[a] Department of Mechanical Engineering, Nan Kai Institute of Technology, Nantou, Taiwan, ROC
[b] Department of Mechanical Engineering, National Chaio Tung University, Hsinchu 30010, Taiwan, ROC

Received 28 June 2006; received in revised form 8 September 2006
Available online 14 November 2006

Abstract

An experiment is conducted here to investigate the saturated flow boiling heat transfer characteristics of ozone friendly refrigerant R-410A in a horizontal annular finned duct. Meanwhile the associated bubble characteristics in the duct are also inspected from the flow visualization. The experimental data are presented in terms of saturated flow boiling curves, boiling heat transfer coefficients and flow photos. In addition, empirical correlation equations for the saturated flow boiling heat transfer coefficient and mean bubble departure diameter are proposed. The saturated flow boiling curves show that boiling hysteresis is insignificant in the flow and the wall superheat needed for the onset of nucleate boiling is slightly affected by the refrigerant mass flux. Besides, the boiling curves are mainly affected by the imposed heat flux and refrigerant mass flux. Moreover, the measured saturated flow boiling heat transfer coefficient increases with the imposed heat flux and refrigerant mass flux. Furthermore, at a higher refrigerant mass flux the departing bubbles are smaller.

1. Introduction

It is well known that refrigerant R-22 is still one of the most widely used HCFCs (hydrochlorofluorocarbons) employed as a working fluid in air conditioning systems. But it will be phased out in a short period of time since the chlorine it contains has high ozone depletion and global warming potentials. Recently, various non-chlorine alternative refrigerants such as R-134a, R-407C and R-410A were proposed to replace R-22 for various applications. In particular, R-410A which is the most widely used ozone depletion free refrigerant is recognized as the main replacement to R-22.

In order to properly use these new refrigerants in the air conditioning and refrigeration systems, the detailed understanding of the two-phase heat transfer and associated bubble characteristics for these new refrigerants is essential. The main purpose of this study is to investigate the saturated flow boiling of refrigerant R-410A in a horizontal annular finned duct by measuring the boiling heat transfer coefficient and visualizing the motion of bubbles in the boiling flow.

In the following the relevant literature on the present study of R-410A saturated flow boiling is reviewed. It should be mentioned here that refrigerant R-410A is a mixture of R-32 and R-125 (50% by mass) which exhibits azeotropic behavior with a small temperature glide of about 0.1 °C. A recent comprehensive review of the literature on the nucleate pool and flow boiling of new refrigerants was conducted by Thome [1]. He assessed the strength and weakness in the existing boiling correlations and in the maps for two-phase flow patterns and identified the further research requirements and objectives. Sami and Poirier [2] compared the evaporation and condensation heat transfer data for several refrigerant blends proposed as substitutes for R-22, including R-410A, R-410B, R-507 and the quaternary mixture R-32/125/143a/134a, inside an enhanced-surface tubing. They showed that the

* Corresponding author. Tel.: +886 35 712121x55118; fax: +886 35 726440.
E-mail address: tflin@mail.nctu.edu.tw (T.F. Lin).

0017-9310/$ - see front matter © 2006 Elsevier Ltd. All rights reserved.
doi:10.1016/j.ijheatmasstransfer.2006.09.009

Nomenclature

A_s, A_{cs}	surface area and cross-sectional area, m^2
b_1, b_2	fin size defined in Fig. 3, m^2
Bo	boiling number, $Bo = \frac{q}{Gi_{fg}}$, dimensionless
c_p	specific heat, J/kg °C
Co	convection number, $Co = \left(\frac{\rho_g}{\rho_f}\right)^{0.5}\left[\frac{1-x}{x}\right]^{0.8}$, dimensionless
d_p	mean bubble departure diameter, m
$\overline{d_p}$	mean non-dimensional bubble departure diameter, dimensionless
D	diameters of annular duct defined in Fig. 3, m
D_h	hydraulic diameter, m
Fr	Froude number, $Fr = \frac{G^2}{\rho_f^2 \cdot g \cdot D_h}$, dimensionless
g	acceleration due to gravity, m/s^2
G	refrigerant mass flux, kg/m^2 s
$h_{r,f}$	liquid convection heat transfer coefficient, W/m^2 °C
$h_{r,sat}$	saturated boiling heat transfer coefficient, W/m^2 °C
i_{fg}	enthalpy of vaporization, J/kg
I	current, A
k	thermal conductivity, W/m °C
l	length, m
p	pitch of fins, m
Pr	Prandtl number, $Pr = \frac{\mu_f \cdot c_{p,f}}{k_f}$, dimensionless
q, q_t	average net heat flux and total imposed heat flux, kW/m^2
Q, Q_t	convection heat transfer rate and total power input to test section, kW
Re	Reynolds number, $Re = \frac{G \cdot D_h}{\mu_f}$, dimensionless
T	temperature, °C
V	voltage, V
x	vapor quality
z	downstream coordinate for annular duct flow, m

Greek symbols

$\Delta\rho$	density difference between liquid and vapor phases, kg/m^3
μ	dynamic viscosity, N s/m^2
ρ	density, kg/m^3
σ	surface tension, N/m

Subscripts

ave	average
f, g	liquid/vapor phase
i, o	inlet/inner, outlet/outer
sat	saturated state
wall	heated wall

two-phase heat transfer coefficients and pressure drops increased with the refrigerant mass flux for all alternative refrigerants and R-22. In a continuing study [3], they presented the data for R-410A and R-507 in a double fluted tube indicating that for the refrigerant Reynolds number higher than 4.2×10^6, R-410A had higher heat transfer rate than R-507. Wang et al. [4] tested nucleate boiling on several commercially available enhanced-surface tubes to assess the pool boiling heat transfer performance for R-22, R-123, R-134a, R-407C, and R-410A. The heat transfer coefficient of R-410A was found to be higher than that of R-22 for most enhanced tubes. This outcome is attributed to the higher latent heat, thermal conductivity and specific heat and lower liquid viscosity for R-410A. Later, they [5] compared the two-phase heat transfer and pressure drop characteristics of refrigerants R-22 and R-410A flowing in a horizontal smooth tube. Their results indicated that the heat transfer coefficients for R-410A were about 10–20% higher than that for R-22 and the pressure drops of R-410A were about 30–40% lower than that of R-22. Ebisu and Torikoshi [6] measured the evaporation heat transfer coefficients and proposed empirical correlations for R-410A, R-407C and R-22 flowing in a horizontal smooth tube. Their results showed that the evaporation heat transfer coefficient of R-410A was about 20% higher than that of R-22 up to the vapor quality of 0.4, while the heat transfer coefficients for R-410A and R-22 became almost the same at the quality of 0.6. Furthermore, the pressure drop for R-410A was about 30% lower than that of R-22 during evaporation. The quantitative differences in the pressure drops between R-410A and R-22 were mainly attributed to the differences in the vapor densities of two refrigerants. The larger the vapor density, the smaller the pressure drop of a refrigerant. Similar study was carried out by Wijaya and Spatz [7] for refrigerants R-22 and R-410A in a horizontal smooth copper tube. Their data showed that the evaporation heat transfer coefficient for R-410A was much higher (about 23–63%) than that for R-22, while the R-410A pressure drop was 23–38% lower than that for R-22. The advantageous heat transfer and pressure drop characteristics for R-410A were ascribed to the better transport properties for R-410A. Shen et al. [8] provided the data for the pool boiling heat transfer coefficient of binary mixture R-32/R-125 with different mole fractions of R-32. The results indicated that the pressure and heat flux dependences of the boiling heat transfer coefficient for the binary mixture did not significantly differ from those of pure components. The frictional pressure characteristics for R-410A flowing in a 5-mm smooth tube reported by Chang et al. [9] showed the substantial increase of the pressure drop gradient with the refrigerant mass flux and vapor quality. Furthermore, they analyzed the frictional pressure drop using the two-phase frictional multiplier. The averaged heat transfer coefficients for forced

convection condensation of R-410A and R-22 inside smooth horizontal tubes were experimentally determined by Chitti and Anand [10]. Their results showed that R-410A had about 15–20% higher regionally averaged heat transfer coefficient when compared to R-22 at a given refrigerant mass flux. They also studied the effects of lubricating oil on the condensation heat transfer characteristics. Recently, Hsieh and Lin [11] measured the saturated flow boiling and pressure drop of R-410A in a vertical plate heat exchanger. Their results indicate that the heat flux exhibits significant effects on the saturated flow boiling heat transfer coefficient.

Based on the available experimental data from the open literature, some correlating equations for flow boiling heat transfer were proposed [12–15]. An early general correlation model for the two-phase flow boiling, which is still widely used, is that of Chen [12]. He divided the boiling heat transfer coefficient into two parts: a microconvective (nucleate boiling) contribution estimated by some pool boiling correlations and a macroconvective (non-boiling forced convection) contribution estimated by some single-phase correlations. In order to account for the diminished contribution of nucleate boiling as the macroconvective effects increased at a higher vapor quality, he introduced the enhanced factor E and suppression factor S to respectively accommodate the forced convective and nucleate boiling contributions. Gungor and Winterton [13] modified the Chen's correlation and proposed the correlations for the enhanced and suppression factors. An enhanced model was developed by Kandlikar [14] to predict the saturated boiling heat transfer coefficients for refrigerants inside horizontal and vertical tubes. A new correlation from Liu and Winterton [15] introduced an asymptotic function to predict the heat transfer coefficients for vertical and horizontal flows in tubes and annuli.

The above literature review clearly reveals that although R-410A is one of the most possible substitutes for R-22, the two-phase boiling heat transfer and associated bubble characteristics for R-410A remain poorly explored. In the present study experiments are conducted to investigate the heat transfer characteristics in the saturated flow boiling of R-410A in a horizontal annular finned duct and to visualize the motion of bubbles in the duct.

2. Experimental apparatus and procedures

The experimental apparatus established in the previous study [16] is modified slightly here to investigate the saturated flow boiling heat transfer of R-410A in a horizontal annular finned duct and is schematically shown in Fig. 1. The apparatus consists of three main loops, namely, the refrigerant, water–glycol and water loops, along with a data acquisition system. Refrigerant R-410A is circulated in the refrigerant loop. We need to control the temperature and flow rate in the water–glycol loop to have enough cooling capacity for condensing the R-410A vapor and subcooling the R-410A liquid to a preset temperature. We further utilize the water loop installed before the test section to procure the preset condition of refrigerant R-410A at the test section inlet. A DC power supply is used for heating the inner pipe in the test section. To obtain the data of the bubble departure size in the R-410A saturated flow boiling in the annular duct, a camera connected to a photographic microscope is set up beside the test section to visualize the boiling flow.

2.1. Refrigerant loop

The refrigerant loop contains a variable-speed refrigerant pump, an accumulator, a mass flow meter, a test section, a condenser, a sub-cooler, a receiver, a filter/dryer and four sight glasses. A rotational DC motor is used to drive the refrigerant pump which then circulates the R-410A liquid from the receiver to the test section. Through changing the DC current in the motor, the liquid flow rate of R-410A can be varied. By adjusting the gate opening of the valve at the downstream of the test section, the pressure of the refrigerant in the test section can be regulated. Note that the refrigerant flow rate and pressure should be adjusted simultaneously in order to control them at the required levels. Moreover, a high-pressure nitrogen tank is installed in the loop to dampen the fluctuations of the flow rate and pressure. The refrigerant flow rate is measured by a mass flow meter with a reading accuracy of 1%. The filter/dryer is used to filter the impurities and non-condensable gas possibly existing in the loop. Meanwhile, the condenser and subcooler are used to condense the R-410A vapor leaving the test section and then the liquid R-410A is subcooled by the cold water–glycol loop. Varying the temperature and flow rate of the water–glycol mixture moving through the condenser and subcooler allows us to control the bulk temperature of R-410A leaving the subcooler. After subcooled, the liquid R-410A flows back to the receiver at the bottom of the system.

2.2. Test section

As schematically shown in Fig. 2, the test section is a horizontal annular finned duct with the outer pipe made of pyrex glass to permit the visualization of boiling processes. The outer pyrex glass pipe is 160 mm long, having a 20-mm inside diameter and 2.5-mm thick wall. Both ends of the pipe are connected with copper tubes by means of flanges and are sealed by O-rings. The inner finned pipe is manufactured from a copper pipe. It is 180 mm long and has 12.7-mm nominal outside diameter. There are helical integral low fins (26 fins/in.) on the outside surface of the inner pipe. The detailed geometrical data of the finned pipe are given in Fig. 3 and Table 1. An electric cartridge heater of 160-mm in length and 7.0-mm in diameter with a maximum power output of 800 W is inserted into the inner finned pipe. Furthermore, the finned pipe has a 10-mm inactive heating zone at each end and is insulated with teflon blocks and the thermally non-conducting epoxy to

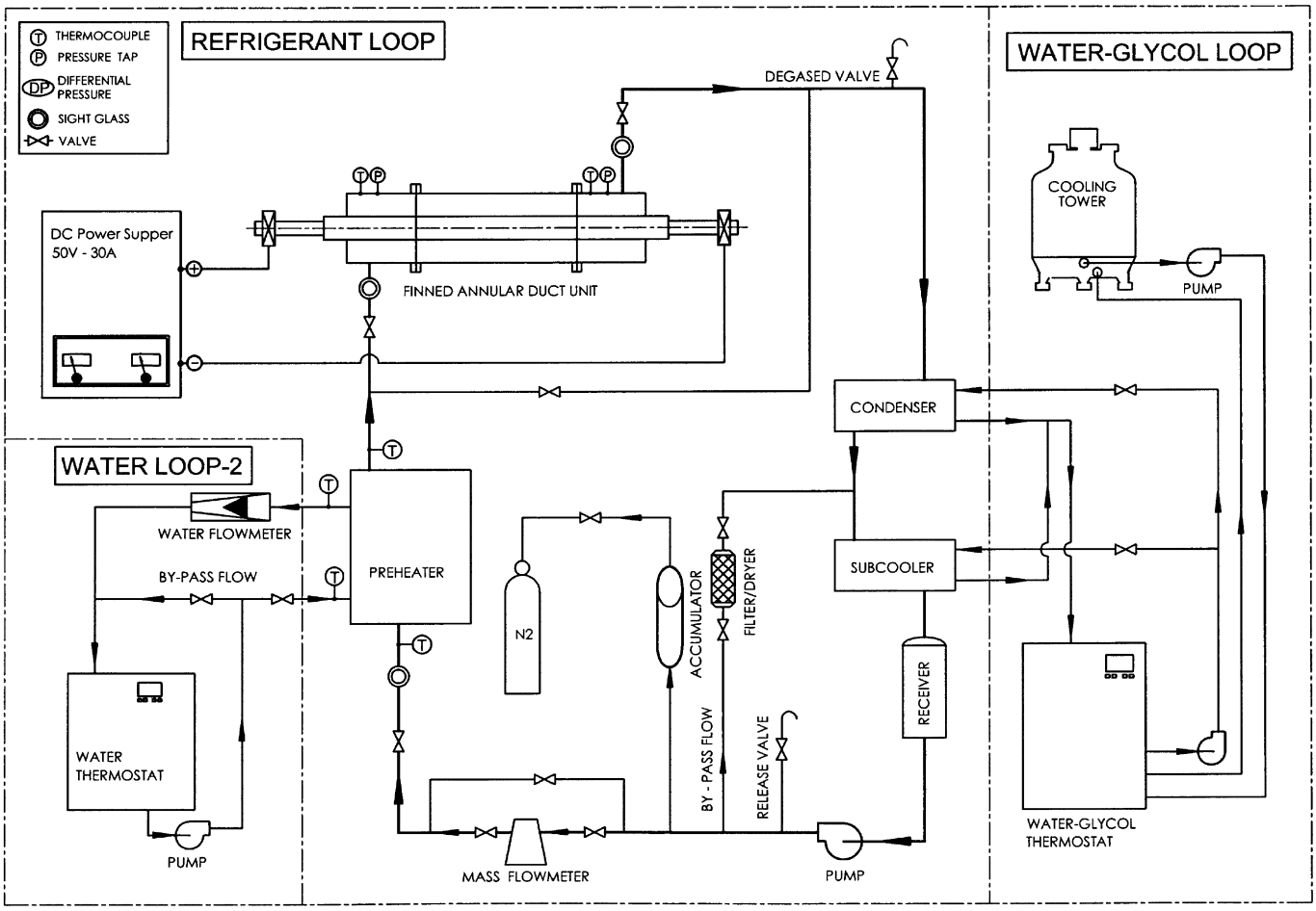

Fig. 1. Schematic diagram of the experimental system for saturated flow boiling in horizontal annular finned duct.

minimize heat loss from it. Thermal contact between the heater and the finned pipe is improved by coating a thin layer of heat-sink compound on the heater before installating the heater. Then, 12 T-type calibrated thermocouples with their beads covered with the electrically non-conducting thermal bond are fixed on the inside surface of the finned pipe so that the voltage signals from the thermocouples are not interfered by the DC current passing through the cartridge heater. The thermocouples are positioned at five axial stations along the finned pipe. At each axial station, two to four thermocouples are placed at top, bottom, or two sides of the pipe circumference with 180° or 90° apart. The outside surface temperature of the finned pipe is then derived from the measured inside surface temperature by taking the radial thermal conduction through the pipe wall into account. Fig. 4 shows the detailed thermocouple locations at each axial station and the arrangement of the cartridge heater.

2.3. DC power supply

As described above, the finned pipe is heated by a 800-W cartridge heater. A 50V-25A DC power supply delivers the required electric current to the cartridge heater. A Yokogawa DC meter is used to measure the dc current through the cartridge heater with an accuracy of 1%. Then the voltage drop across the heater is measured by a Yokogawa multimeter. Thus the power input to the heater can be calculated.

2.4. Photographic system

The photographic apparatus established in the present study to unravel the bubble characteristics in the saturated flow boiling in the annular finned duct consists of a Kodak Motion Corder Analyzer and a Nikon 85-mm microlens camera. The high-speed motion analyzer system can take photographs up to 10,000 frames/s. Here, a recording rate of 1000 frames/s is used to obtain the images of bubble ebullition processes in the flow boiling. The bubble dynamics data are collected at three different axial locations along the flow direction ($z/D_h = 6$, 12 and 18). After the system reaches a statistically steady state, we record the boiling activity. The high-speed motion analyzer stores the images which are later downloaded to a tape to facilitate the playback at slower motion (15 frames/s) on a CRT. Then, the bubble departure diameter is calculated by viewing more than 500 frames at each location. In order to achieve the

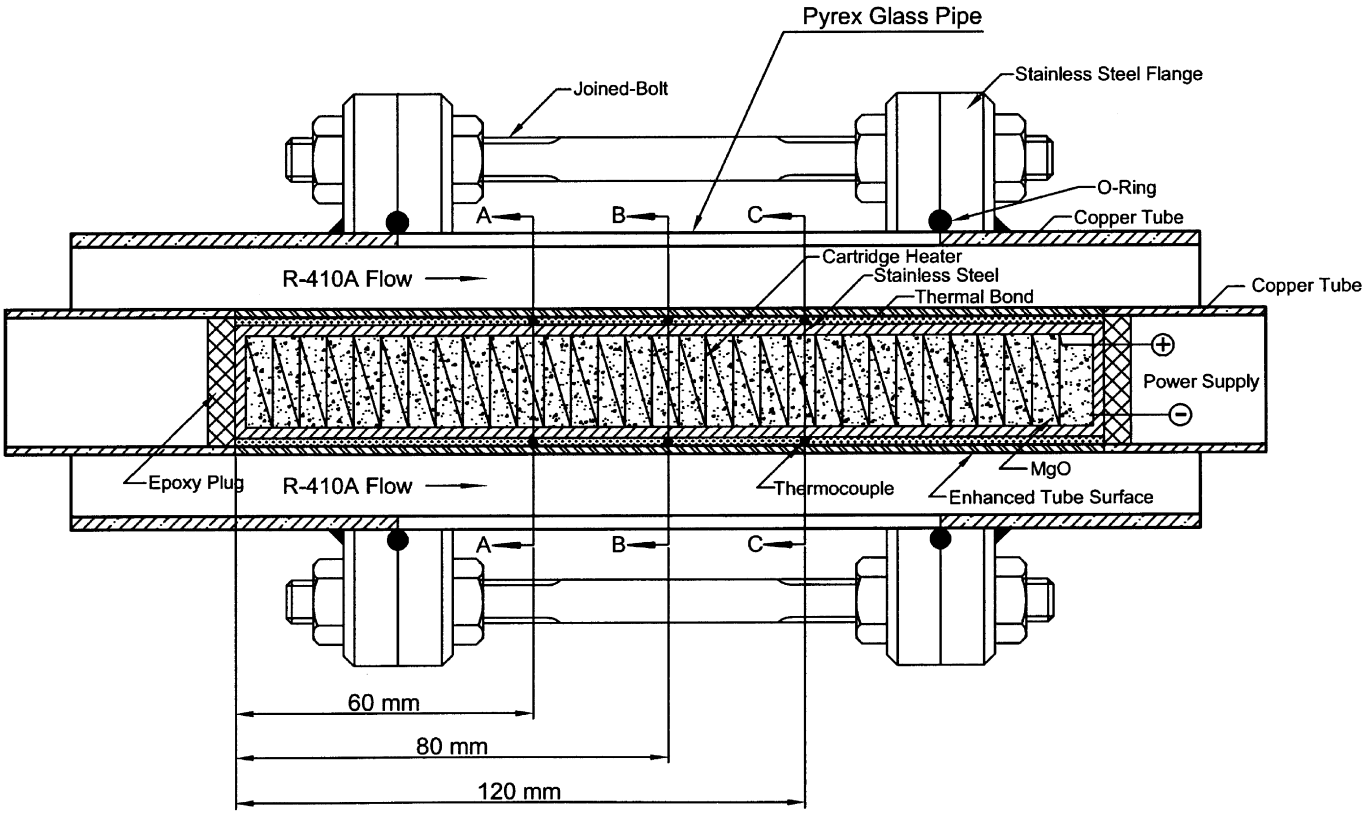

Fig. 2. Schematic diagram of the test section for saturated flow boiling in horizontal annular finned duct.

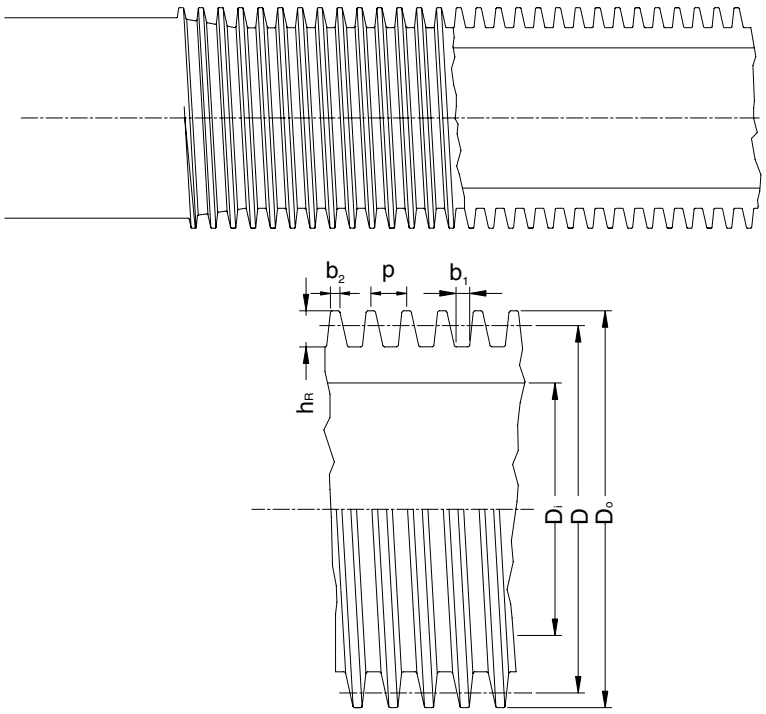

Fig. 3. Schematic diagram of inner finned pipe.

highest possible resolution and eliminate errors in calibration, the camera lens is fixed at a constant focal length, resulting in a fixed viewing area of approximately 5-fin-pitch length (corresponding to an image field area of 5.5×4.5 mm). Typically, a total of over 150 bubble diameter measurements is used to construct the present data.

Table 1
Specifications of the inner finned duct

Items	Specifications
Geometry type	Helical integral low fins
Finned pipe diameter, D_o (mm)	12.7
Nominal outside diameter, D (mm)	11.5
Nominal inside diameter, D_i (mm)	8.0
Number of fins, N (fins/in.)	26
Fin pitch, p (mm)	0.98
Fin height, h_R (mm)	1.3
Finned thickness (base), b_1 (mm)	0.45
Finned thickness (tip), b_2 (mm)	0.25
Helix angle, α (deg)	5.0
Fin included angle, β (deg)	25
Actual heat-transfer area, A_{as} (m^2/m)	0.098
Tube length, l (mm)	160

2.5. Water–glycol mixture loop

The water–glycol loop designed for condensing the R-410A vapor and for subcooling the liquid R-410A contains a 125-l constant temperature bath with a water cooled refrigeration system. The cooling capacity is 2 kW for the water–glycol mixture at −20 °C. The cold water–glycol mixture at a specified flow rate is driven by a 0.5-hp pump to the condenser as well as to the subcooler. A by-pass loop is provided to adjust the flow rate. By adjusting the mixture temperature and flow rate, the bulk temperature of the R-410A in the subcooler can be controlled at a preset level.

2.6. Water loop for preheater

In order to have a better control of the R-410A temperature at the test section inlet, a water loop is used to preheat the R-410A before it arrives at the test section inlet. This water loop consists of a 20-l water thermostat with a 0.5-kW heater and an air cooled refrigeration unit of 0.5-kW cooling capacity. A 0.5-hp water pump is used to drive the hot water at a specified temperature to the heat exchanger of the preheater at a specified water flow rate. A by-pass valve can also be used to adjust the water flow rate. The reading accuracy of measuring the water flow rate is ±0.5%.

2.7. Data acquisition

The data acquisition system includes a recorder, a 24V-3A power supply and a computer. The recorder is used to record the temperature and voltage data. The water flowmeter and differential pressure transducer need the power supply as a driver to output an electric current of 4–20 mA. The IEEE 488 interface is used to connect the computer with the recorder, allowing the measured data to be transmitted from the recorder to the computer and then analyzed immediately. The system automatically monitors 22 copper–constantan thermocouples, two pressure transducers, and two mass flowmeters.

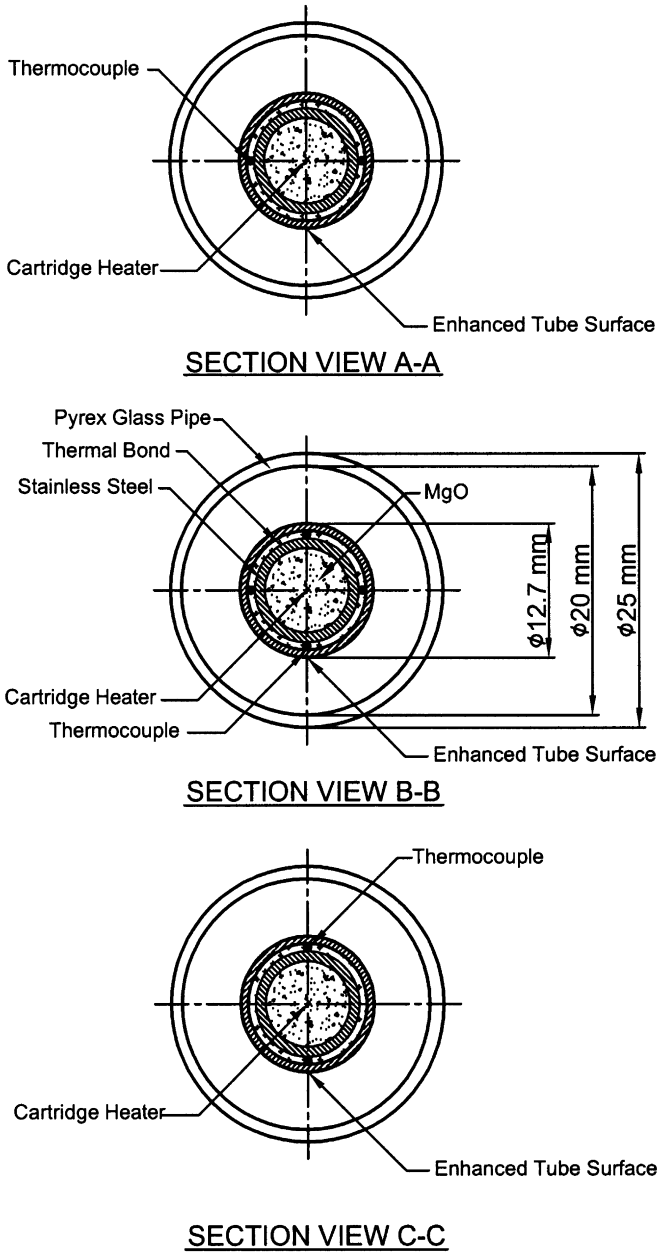

Fig. 4. Detailed cross-section of the cartridge heater and thermocouple locations.

2.8. Experimental procedures

In the test the R-410A liquid at the inlet of the test section is first maintained at a specified temperature by adjusting the water–glycol temperature and flow rate. In addition, we adjust the thermostat temperature in the water loop to obtain the saturated liquid R-410A at the test section inlet. Then, we regulate the R-410A pressure at the test section inlet by adjusting the gate valve locating right after the exit of the test section. Meanwhile, the current of the DC motor connecting with the refrigerant pump is selected to obtain the required R-410A flow rate. The imposed heat flux from the heater to the R-410A is adjusted by varying

Table 2
Summary of the uncertainty analysis

Parameter	Uncertainty
Annular finned duct geometry	
Length, diameter (m)	±0.00005
Area (m^2)	$\pm 7 \times 10^{-5}$
Sensors	
Temperature, T (°C)	±0.2
Temperature difference, ΔT (%)	±4.5%
System pressure, P (MPa)	±0.002
Pressure drop, ΔP (Pa)	±200
Water flow rate, W_w (%)	±2
Mass flux of refrigerant, G (%)	±2
Single-phase heat transfer	
Heat transfer rate, q (%)	±6.5
Heat transfer coefficient, $h_{r,f}$ (%)	±11
Saturated flow boiling heat transfer	
Boiling heat flux, q (%)	±6.5
Heat transfer coefficient, $h_{r,sat}$ (%)	±14.5

the electric current delivered from the DC power supply. By measuring the current delivered to and voltage drop across the heater, we can calculate the heat transfer rate to the refrigerant.

2.9. Uncertainty analysis

The uncertainties of the experimental results are analyzed by the procedures proposed by Kline and McClintock [17]. The detailed results from the present uncertainty analysis for the experiments conducted here are summarized in Table 2.

3. Data reduction

A data reduction analysis is needed to calculate the saturated flow boiling heat transfer coefficient from the raw data measured in the horizontal annular finned duct. The data reduction process is described in the following.

The imposed heat flux was calculated on the basis of the total power input and the outside surface area of the inner pipe. The total electrical power input to the test section was computed from the product of the measured voltage drop across the cartridge heater and the electric current passing through it. The imposed heat flux at the outside surface of the inner pipe based on the total power input is evaluated from

$$q_t = \frac{V \cdot I}{A_s} \tag{1}$$

where V and I respectively represent the measured voltage drop and current. The outside surface area of the inner finned pipe A_s is used in Eq. (1) and is equal to $\pi D_o l$, where D_o is the outer diameter of the pipe (Fig. 3) and l is the length of the inner pipe ($l = 160$ mm). Before the flow boiling experiments, the total heat loss from the test section was inspected by comparing the total power input from the power supply with the enthalpy increase in the single-phase liquid refrigerant flow which can be expressed as

$$Q = G \cdot A_{cs} \cdot c_{p,f} \cdot (T_o - T_i) \tag{2}$$

where A_{cs} is the cross-sectional area of the annular duct, and T_o and T_i are respectively the refrigerant temperatures at the exit and inlet of the test section. The results from this heat loss test indicated that the relative heat loss from the test section, $\varepsilon = (Q_t - Q)/Q_t$, was generally less than ±4% of the total power input Q_t.

The average saturated flow boiling heat transfer coefficient of R-410A in the annular duct from the present experiments is defined as

$$h_{r,sat} = \frac{q}{(T_{wall} - T_{sat})} \tag{3}$$

where q is the net imposed heat flux to the R-410A flow and is estimated by $q = q_t \cdot (1 - \varepsilon)$. T_{sat} is the saturated temperature corresponding to the test pressure. Note that T_{wall}

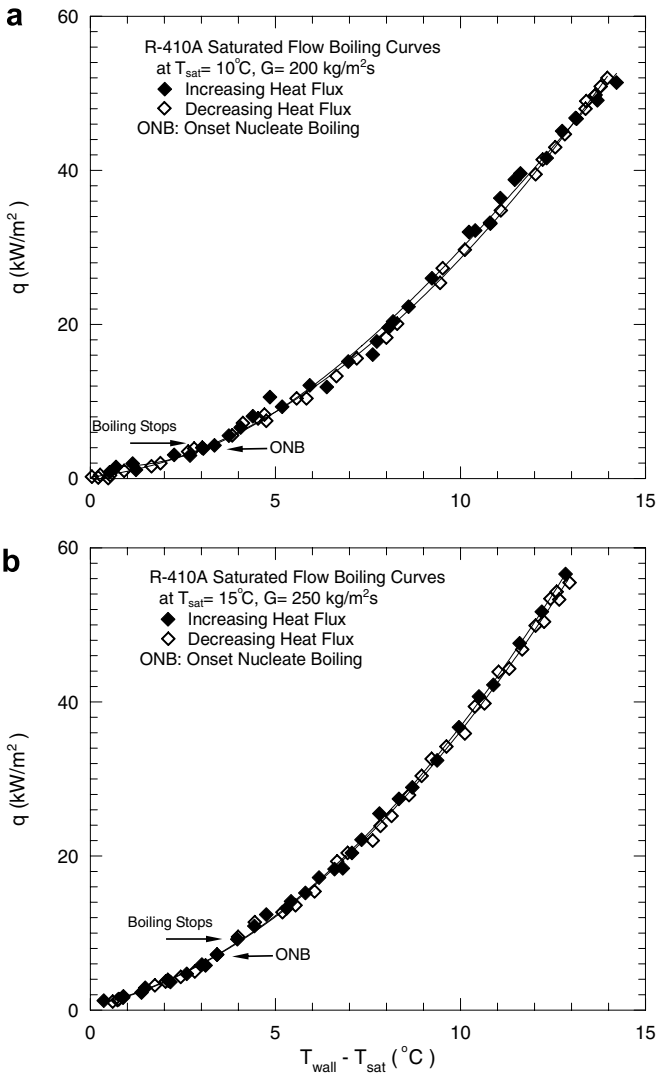

Fig. 5. Boiling curves showing the degree of hysteresis effect during the saturated flow boiling at (a) $T_{sat} = 10$ °C, $G = 200$ kg/m^2 s and (b) $T_{sat} = 15$ °C, $G = 250$ kg/m^2 s.

denotes the average outside surface temperature of the inner pipe. The outside surface temperature $T_{wall,o}$ at each thermocouple location is deduced from the measured inside surface temperature $T_{wall,i}$ of the pipe by subtracting the radial temperature drop due to the radial heat conduction in the pipe wall. Thus we have

$$T_{wall,o} = T_{wall,i} - Q\frac{\ln(D_0/D_i)}{2\pi k_{wall} \cdot l} \quad (4)$$

In this evaluation of $T_{wall,o}$ the axial conduction in the pipe wall is assumed to be small compared with the radial conduction. More specifically, T_{wall} is then considered as the arithmetic average of the deduced outside surface temperatures of the inner pipe from the thermocouple data.

4. Results and discussion

The present saturated flow boiling experiments are conducted for the refrigerant mass flux varying from 150 to 250 kg/m^2 s, imposed heat flux from 0 to 50 kW/m^2 and refrigerant saturated temperature from 5 to 15 °C (corresponding to the saturation pressure from 0.93 to 1.25 MPa). Selected data from the experiments are presented here to illustrate the characteristics of the heat transfer and bubble motion in the saturated flow boiling of R-410A in the horizontal annular finned duct. Specifically, the effects of the imposed heat flux, refrigerant mass flux and saturated temperature on the measured boiling curves and heat transfer coefficients and bubble characteristics will be examined in detail. In addition, empirical correlation equations for the flow boiling heat transfer coefficients and bubble departure diameter are proposed.

4.1. Boiling curves

The possible presence of the boiling hysteresis is examined first in Fig. 5 by presenting the data for the boiling

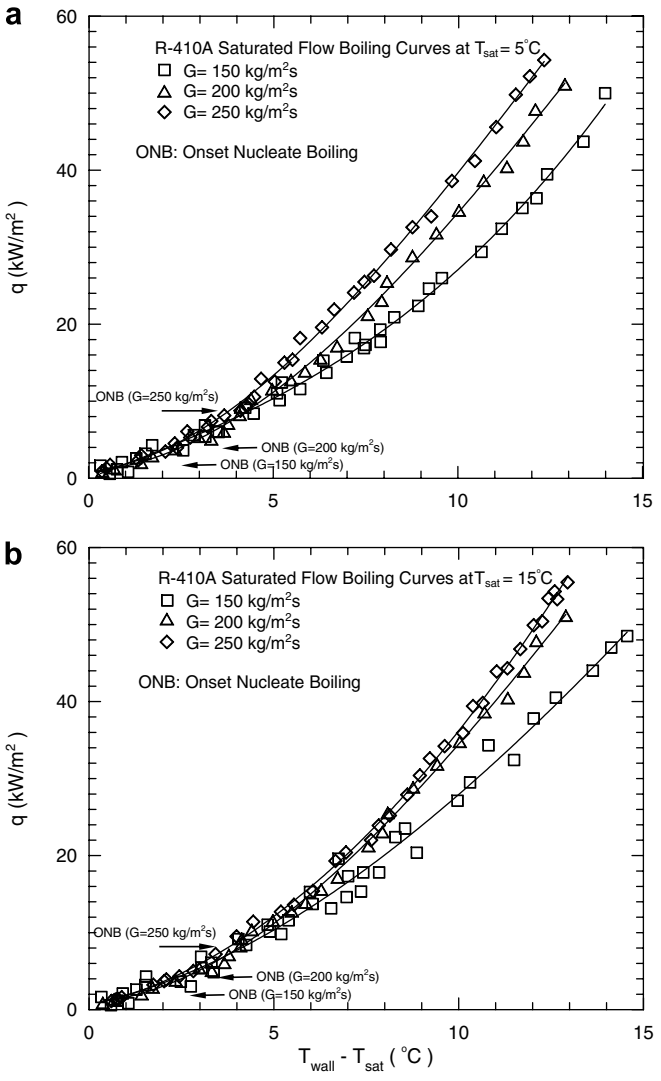

Fig. 6. Saturated flow boiling curves for various refrigerant mass fluxes ($G = 150$, 200 and 250 kg/m^2 s) at (a) $T_{sat} = 5$ °C and (b) $T_{sat} = 15$ °C.

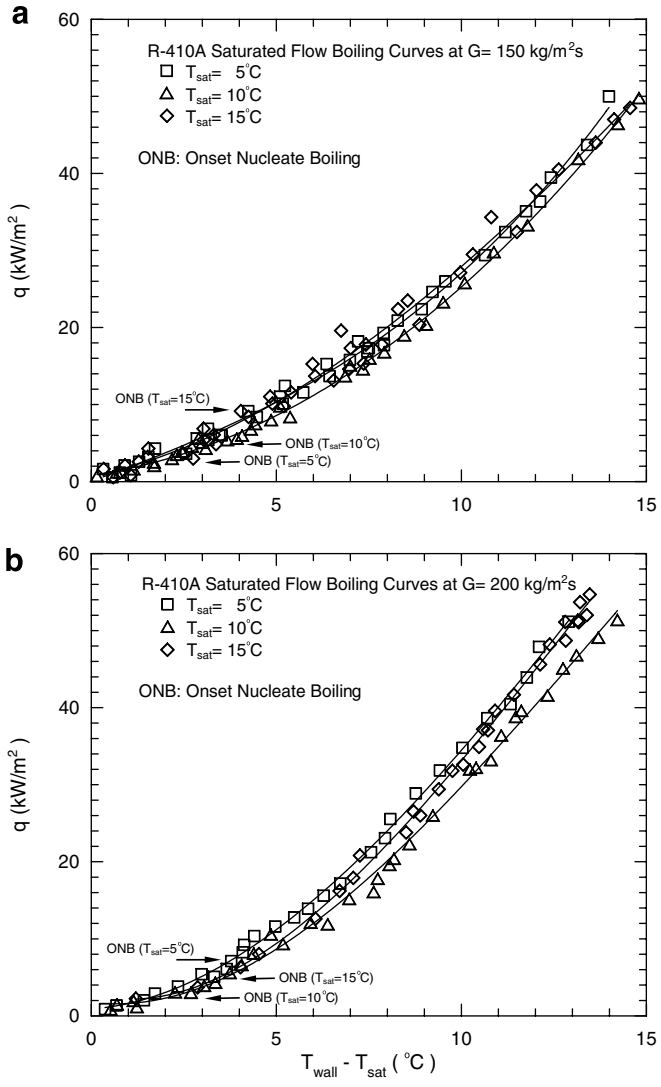

Fig. 7. Saturated flow boiling curves for various saturated temperatures ($T_{sat} = 5$, 10 and 15 °C) at (a) $G = 150$ kg/m^2 s and (b) $G = 200$ kg/m^2 s.

curves measured at the middle axial location ($z = 80$ mm) for the cases with $T_{sat} = 10$ °C and $G = 200$ kg/m^2 s and $T_{sat} = 15$ °C and $G = 250$ kg/m^2 s. The results show that for each case the wall superheat ($T_{wall} - T_{sat}$) increases almost exponentially with the imposed heat flux q. Moreover, the boiling curves for the increasing and decreasing imposed heat fluxes almost overlap. Apparently, the boiling hysteresis and the temperature undershoot at the onset of nucleate boiling (ONB) are small for the saturated flow boiling in this annular finned duct. The smaller boiling hysteresis and temperature undershoot are considered to mainly result from the fact that most of cavities are activated on the fin surface in the saturated flow boiling even at the low imposed heat flux of $q = 5$ kW/m^2. It is worth mentioning that the hysteresis and temperature undershoot in the horizontal smooth duct are relatively significant [18]. Besides, the condition for the ONB is difficult to determine from the data in the measured boiling curves since the slope change in the boiling curves during the ONB is very small. Hence, the ONB is determined here from the flow visualization.

Next, the effects of the refrigerant mass flux and saturated temperature on the saturated flow boiling heat transfer of R-410A in the horizontal annular finned duct are illustrated in Figs. 6 and 7 by presenting the boiling curves for various G at a fixed T_{sat} and for various T_{sat} at a fixed G. The results in Fig. 6 manifest that at low wall superheat for $\Delta T_{sat} < 5$ °C the boiling curves are only slightly affected by the refrigerant mass flux. From the flow visualization, we noted that in the initial stage of heating the pipe wall, the wall temperature rose slowly but was below that needed for the ONB. Hence no bubble appears on the heating surface. Heat transfer in the flow results completely from the single-phase forced convection. As the imposed wall heat flux was raised gradually, the wall temperature increased correspondingly. At a certain wall superheat a few bubbles started to nucleate from the heating surface and we had onset of nucleate boiling in the

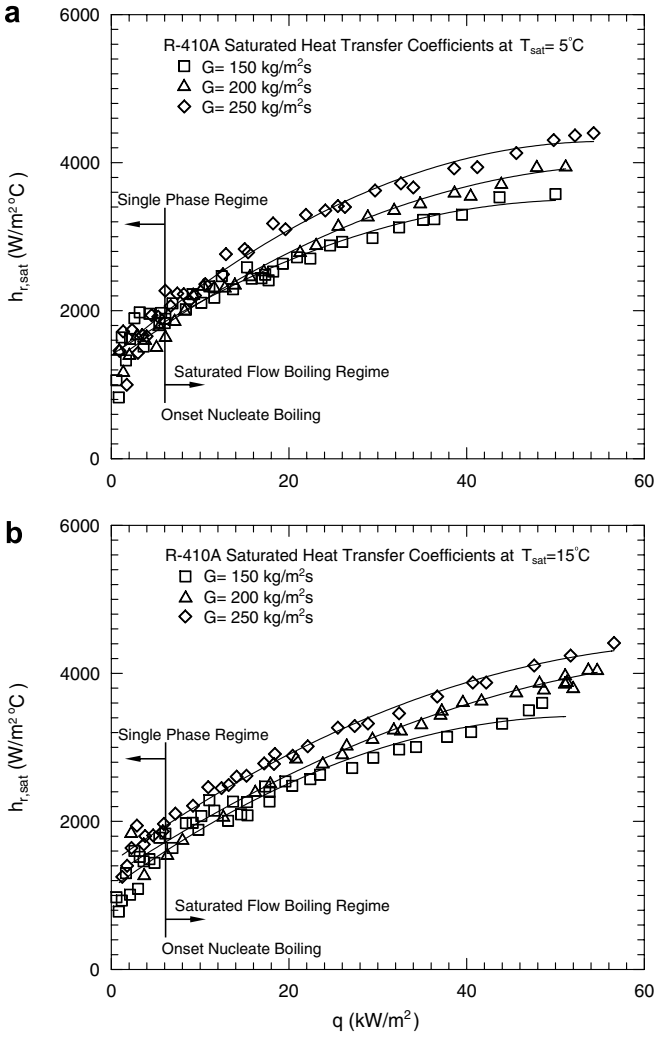

Fig. 8. Variations of saturated flow boiling heat transfer coefficient with imposed heat flux for various refrigerant mass fluxes ($G = 150$, 200 and 250 kg/m^2 s) at (a) $T_{sat} = 5$ °C and (b) $T_{sat} = 15$ °C.

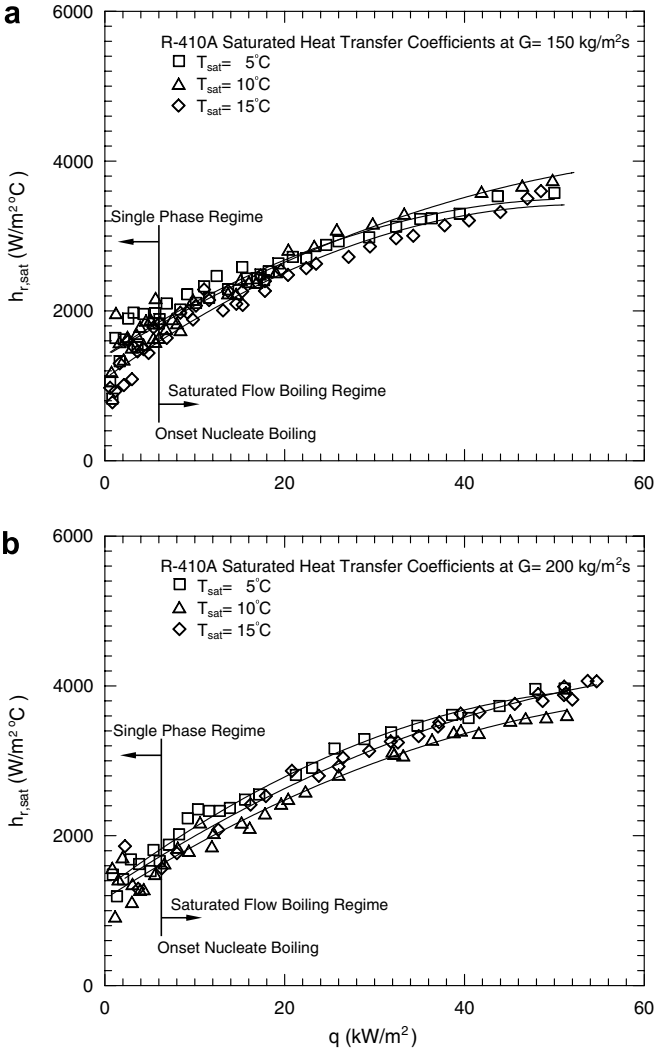

Fig. 9. Variations of saturated flow boiling heat transfer coefficient with imposed heat flux for various saturated temperatures ($T_{sat} = 5$, 10 and 15 °C) at (a) $G = 150$ kg/m^2 s and (b) $G = 200$ kg/m^2 s.

flow. Beyond the ONB, the bubble departure frequency increases significantly with the imposed heat flux, which causes a substantial increase in the heat transfer rate from the wall to the refrigerant. We further noted that at a slightly higher wall superheat for $\Delta T_{sat} > 5$ °C the heat transfer rate from the heating surface to the refrigerant increased with the refrigerant mass flux for $T_{sat} = 5$ °C (Fig. 6a). Besides, the bubbles in the liquid refrigerant moved vigorously and turbulently due to the higher refrigerant mass flux. At an even higher wall superheat for $\Delta T_{sat} > 8$ °C the heat transfer in the R-410A saturated flow boiling is noticeably better at higher refrigerant mass flux. The increase is more prominent at a higher wall superheat. This increase in the heat transfer rate with the mass flux is primarily due to the increasing single-phase convection in the boiling flow with the increasing mass flux. The results from Fig. 6 also indicate that the wall superheat at the ONB is only slightly influenced by the change in the mass flux. The wall superheat at the ONB is about 3–4 °C which is much lower than that in smooth tube [18]. However, the imposed heat flux needed for the ONB is somewhat higher at the higher refrigerant mass flux.

Finally, we note from Fig. 7 that even at the high mass flux of 200 kg/m^2 s the refrigerant saturated temperature only has relatively slight effects on the boiling curves. At the lower G of 150 kg/m^2 s the effects of T_{sat} can be ignored (Fig. 7a). It is further noted that the wall superheat and imposed heat flux at the ONB are somewhat affected by the refrigerant saturated temperature. But the effects of T_{sat} on ΔT_{sat} and q_{ONB} do not exhibit a monotonic trend.

4.2. Saturated flow boiling heat transfer coefficient

The variations of the saturated flow boiling heat transfer coefficient with the imposed heat flux are shown in Figs. 8 and 9 for various refrigerant mass fluxes and saturated temperatures.

The results in Fig. 8 indicate that at given G and T_{sat} both the single-phase forced convection and saturated flow boiling heat transfer coefficients increase with the imposed heat flux. Beyond the ONB, the increase in the boiling heat transfer coefficient is rather significant at increasing imposed heat flux. For example, at $G = 200$ kg/m^2 s and $T_{sat} = 5$ °C the average saturated boiling heat transfer coefficient for $q = 50$ kW/m^2 is about 85% higher than that for

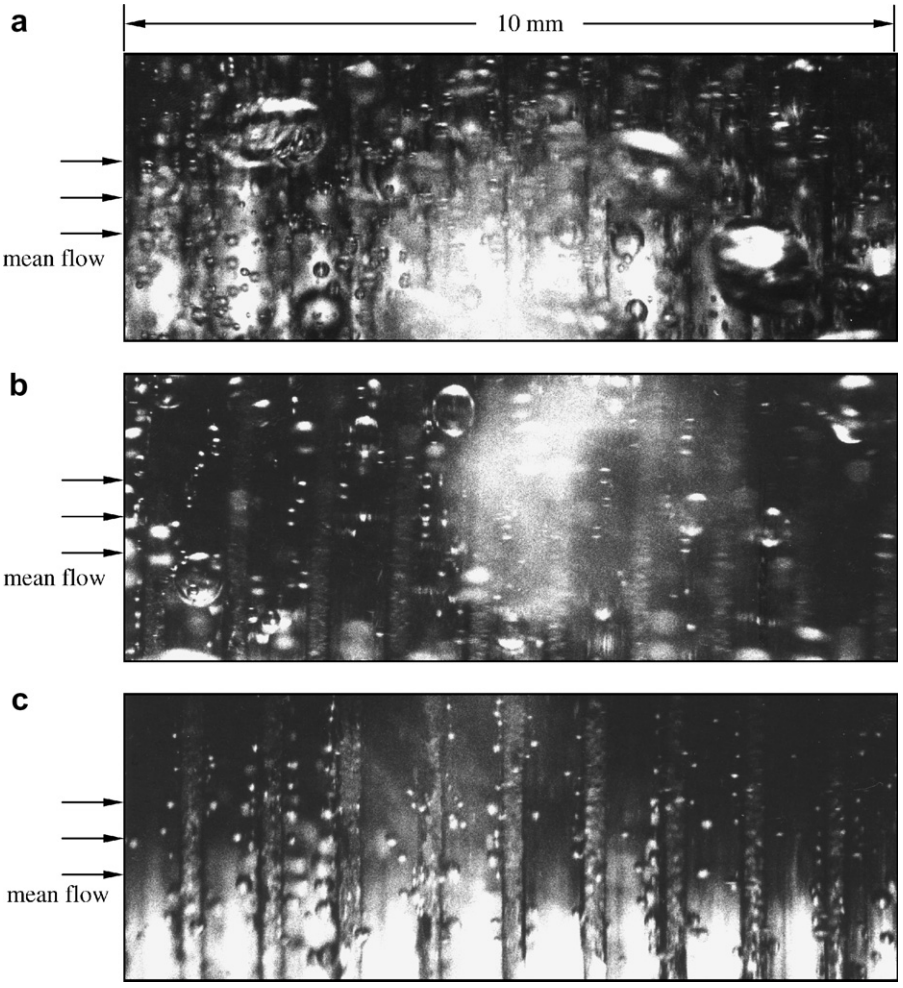

Fig. 10. Photos of bubbles in the saturated flow boiling of R-410A around $z = 80$ mm for $T_{sat} = 15$ °C and $q = 10$ kW/m^2 for (a) $G = 100$ kg/m^2 s, (b) $G = 150$ kg/m^2 s and (c) $G = 250$ kg/m^2 s.

$q = 10$ kW/m^2 (Fig. 8a). This large increase in the saturated flow boiling heat transfer coefficient is ascribed to the higher nucleation density on the heating surface, higher bubble departure frequency and faster bubble growth for a higher imposed heat flux. It is further noted that at a high imposed heat flux for $q > 40$ kW/m^2 the increase of $h_{r,sat}$ with the heat flux becomes much slower. Furthermore, a higher refrigerant mass flux always results in a somewhat higher saturated flow boiling heat transfer coefficient. For instance, the average saturated flow boiling heat transfer coefficient over the entire heat flux range at $T_{sat} = 15$ °C for $G = 250$ kg/m^2 s is respectively about 25% and 8.5% higher than those for $G = 150$ and 200 kg/m^2 s (Fig. 8b).

Finally, it is noted from Fig. 9 that the variations of the saturation flow boiling heat transfer coefficient with the saturated temperature of the refrigerant is within the experimental uncertainty. Hence the effects of T_{sat} on $h_{r,sat}$ can be neglected.

4.3. Bubble characteristics

To illustrate the characteristics of bubbles associated with the R-410A saturated flow boiling in the horizontal annular finned duct, the photos taken for the cases at different refrigerant mass fluxes and imposed heat fluxes from a small region around the middle axial location at $z = 80$ mm are shown in Figs. 10 and 11.

A closed inspection of the photos in Fig. 10 indicates that at a higher mass flux the bubble population is less on the heating surface. The results suggest that at a higher mass flux the liquid refrigerant moves at a higher speed, which in turn tends to sweep the bubbles more quickly away from the heating surface and the vapor condensation inside the bubbles is quicker. Thus, on the heating surface the bubbles are smaller and isolated. Besides, at a higher G the bubble departure frequency is higher and the bubbles are in violent agitating motion. Obviously, a higher refrigerant mass flux results in a smaller bubble departing diameter. Note that at the low mass flux the bubble coalescence is important and a number of big bubbles form in the duct.

How the imposed heat flux affects the bubble characteristics is presented in Fig. 11 for three typical cases with $q = 10$, 15 and 20 kg/m^2 at $G = 150$ kg/m^2 s and $T_{sat} = 5$ °C. The photos show that the effects of the imposed heat flux on the bubble characteristics in the saturated flow

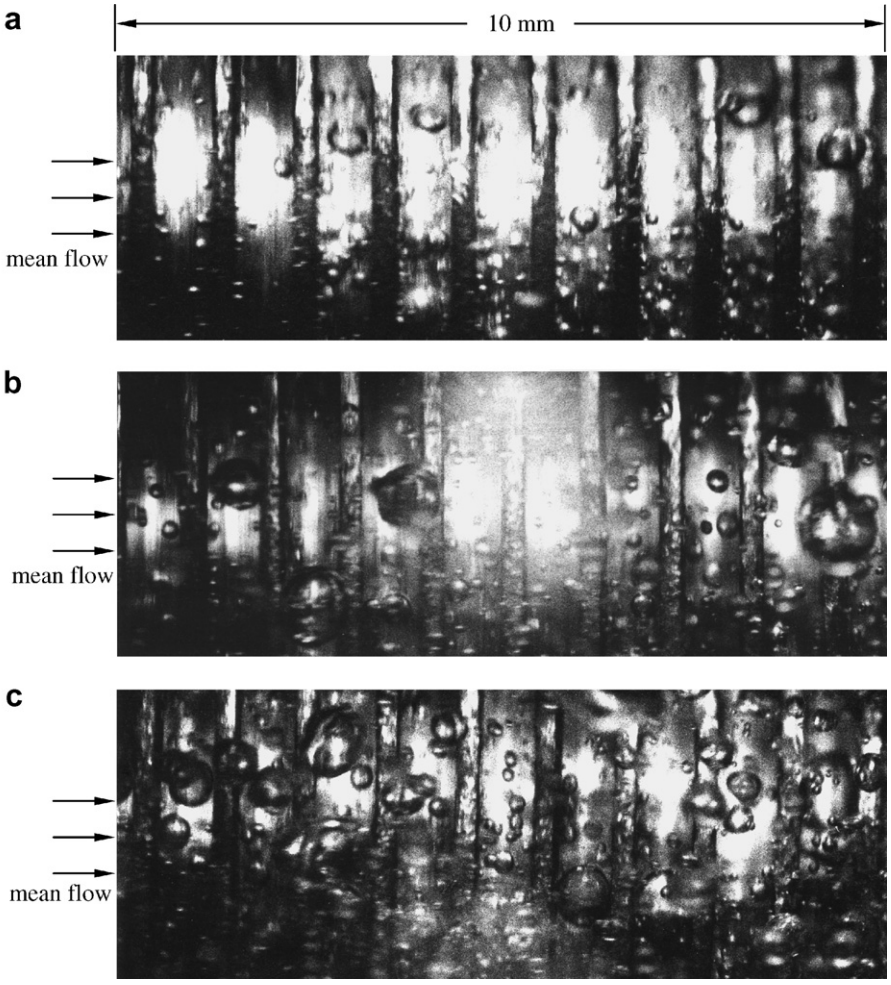

Fig. 11. Photos of bubbles in the saturated flow boiling of R-410A around $z = 80$ mm for $T_{sat} = 5$ °C and $G = 150$ kg/m^2 s for (a) $q = 10$ kW/m^2, (b) $q = 15$ kW/m^2 and (c) $q = 20$ kW/m^2.

boiling is rather significant. A higher wall superheat results from the higher imposed heat flux, which in turn results in a larger number of active nucleation sites and a higher bubble generation frequency. Thus, the corresponding boiling heat transfer from the surface is better. Moreover, at a high imposed heat flux a large number of bubbles generated from cavities in the heating surface tend to coalesce to form large bubbles. At even higher imposed heat flux for $q > 20\ \mathrm{kW/m^2}$, the bubble departure frequency is very high and the bubble coalescence occurs rather frequently so that it is difficult to distinguish the individual bubbles. It should be mentioned that at a high heat flux for $q > 20\ \mathrm{kW/m^2}$ a large number of big bubbles form and they may obstruct the flow space between the fins. This will slow the small bubbles to escape from the heating surface and the liquid refrigerant to rush to the heating surface. Hence, the boiling heat transfer can be retarded by increasing the imposed heat flux for a sufficiently high q ($>50\ \mathrm{kW/m^2}$).

4.4. Correlation equations

An empirical equation to correlate the present data of the heat transfer coefficient for the saturated flow boiling of R-410A in the horizontal annular finned duct is proposed here. The proposed correlation is modified from that of Kandlikar [14] and can be expressed as

$$h_{r,sat} = h_{r,f} \cdot [1.25 \cdot Co^{-0.5} \cdot Fr^{0.35} + 0.95 \cdot Bo^{0.625}] \quad (5)$$

here $h_{r,f}$ is the all-liquid non-boiling heat transfer coefficient and is determined from the empirical correlation for the previous single-phase heat transfer tests for liquid R-410A. It can be expressed as [18]

$$h_{r,f} = 0.2092 \cdot \left(\frac{k_f}{D_h}\right) \cdot Re^{0.78} \cdot Pr^{1/3} \cdot \left(\frac{\mu_{ave}}{\mu_{wall}}\right)^{0.14} \quad (6)$$

In the above equation Co, Fr and Bo are respectively the convection, Froude and boiling numbers, defined as

$$Co = \left(\frac{\rho_g}{\rho_f}\right)^{0.5} \cdot \left[\frac{(1-x)}{x}\right]^{0.8} \quad (7)$$

$$Fr = \frac{G^2}{\rho_f^2 \cdot g \cdot D_h} \quad (8)$$

and

$$Bo = \frac{q}{G \cdot i_{fg}} \quad (9)$$

The empirical correlation proposed above can correlate the present data for $h_{r,sat}$ with an average deviation of 10.6% (Fig. 12). Besides, most data fall within ±20% of the correlation. Then, the mean bubble departure diameter in the saturated flow boiling of R-410A in the horizontal annular finned duct estimated from the present flow visualization can be correlated as

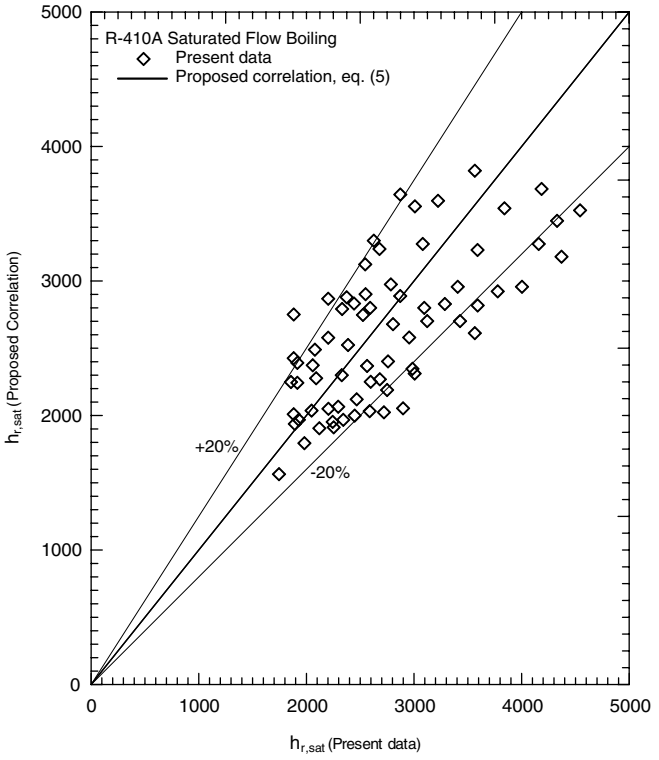

Fig. 12. Comparison of the measured data for heat transfer coefficient in the saturated flow boiling of R-410A with the proposed correlation.

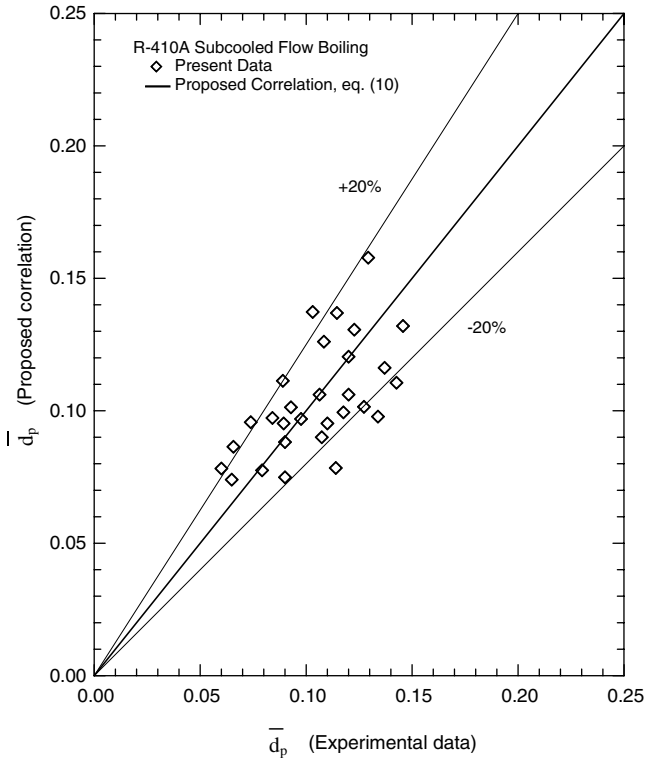

Fig. 13. Comparison of the measured data for mean bubble departure diameter in the saturated flow boiling of R-410A with the proposed correlation.

$$\overline{d_p} \equiv \frac{d_p}{\sqrt{\sigma/(g\Delta\rho)}} = \frac{0.065 \cdot \left(\frac{\rho_f}{\rho_g}\right)^{0.667}}{Re^{0.75} \cdot Bo^{0.5}} \quad (10)$$

Fig. 13 also shows that most of the present experimental data fall within ±20% of the above correlation with an average deviation of 16.1%.

5. Concluding remarks

Experimental measurement has been conducted to investigate the heat transfer characteristics of the saturated flow boiling of R-410A in a horizontal annular finned duct. Results for the heat transfer coefficient and associated bubble characteristics were examined in detail. In addition, empirical equations to correlate the measured heat transfer coefficient and mean bubble departure diameter were proposed. The major results can be summarized in the following.

(1) The boiling hysteresis and the temperature undershoot at ONB are insignificant for the saturated flow boiling in the horizontal annular finned duct which is rather different from that in the smooth duct.
(2) The effects of the imposed heat flux and refrigerant mass flux on the boiling curves are stronger than that of refrigerant saturated temperature. Raising the imposed heat flux and refrigerant mass flux can cause a substantial increase in the boiling heat transfer coefficient.

Acknowledgments

The financial support of this study by the engineering division of National Science Council of Taiwan, ROC through the contract NSC 93-2212-E-009-005 is greatly appreciated.

References

[1] J.R. Thome, Boiling of new refrigerants: a state-of-the art review, Int. J. Refrig. 19 (1996) 435–457.
[2] S.M. Sami, B. Poirier, Comparative study of heat transfer characteristics of new alternatives to R-22, ASHRAE Trans. 120 (1997) 824–829.
[3] S.M. Sami, B. Poirier, Two phase flow heat transfer of binary mixtures inside enhanced surface tubing, Int. Common. Heat Mass Transfer 25 (1998) 763–773.
[4] C.C. Wang, W.Y. Shieh, Y.J. Chang, Nucleate boiling performance of R-22, R-123, R-134a, R-410A and R407C on smooth enhanced tubes, ASHRAE Trans. 121 (1998) 1314–1321.
[5] C.C. Wang, J.G. Yu, P.L. Shieh, D.C. Lu, An experimental study of convective boiling of refrigerants R-22 and R-410A, ASHRAE Trans. 121 (1998) 1144–1150.
[6] T. Ebisu, K. Torikoshi, Heat transfer characteristics and correlations for R-410A flowing inside a horizontal smooth tube, ASHRAE Trans. 121 (1998) 556–561.
[7] H. Wijaya, M.W. Spatz, Two-phase flow heat transfer and pressure drop characteristics of R-22 and R-32/R125, ASHRAE Trans. 118 (1995) 1020–1027.
[8] J. Shen, K. Spindler, E. Hahne, Pool boiling heat transfer of refrigerant mixtures R-32/125, Int. Comm. Heat Mass Transfer 26 (1999) 1091–1102.
[9] Y.J. Chang, S.K. Chiang, T.W. Chung, C.C. Wang, Two-phase frictional characteristics of R-410A and air–water in a 5 mm smooth tube, ASHRAE Trans. 123 (2000) 792–797.
[10] M.S. Chitti, N.K. Anand, Condensation heat transfer inside smooth horizontal tube for R-22 and R-32/R-125 mixture, HVAC&R Res. 2 (1996) 79–103.
[11] Y.Y. Hsieh, T.F. Lin, Saturated flow boiling heat transfer and pressure drop of refrigerant R-410A in a vertical plate heat exchanger, Int. J. Heat Mass Transfer 45 (2002) 1033–1044.
[12] J.C. Chen, A correlation for boiling heat transfer to saturated fluids in convective flow, Ind. Eng. Chem. Proc. Des. Dev. 5 (1966) 322–329.
[13] K.E. Gungor, R.H.S. Winterton, A general correlation for flow boiling in tubes and annuli, Int. J. Heat Mass Transfer 29 (1986) 351–358.
[14] S.G. Kandlikar, A general correlation for saturated two-phase flow boiling heat transfer inside horizontal and vertical tubes, ASME J. Heat Transfer 112 (1990) 219–228.
[15] Z. Liu, R.H.S. Winterton, A general correlation for saturated and subcooled flow boiling in tubes and annuli, based on a nucleate pool boiling equation, Int. J. Heat Mass Transfer 34 (1991) 2759–2766.
[16] C.P. Yin, Y.Y. Yan, T.F. Lin, B.C. Yang, Subcooled flow boiling heat transfer of R-134a and bubble characteristics in a horizontal annular duct, Int. J. Heat Mass Transfer 43 (2000) 1885–1896.
[17] S.J. Kline, F.A. McClintock, Describing uncertainties in single-sample experiments, Mech. Eng. 75 (1) (1953) 3–12.
[18] C.H. Chen, Experimental of flow boiling and evaporation heat transfer of R-410A and bubble characteristics in horizontal annular duct, MS. thesis, National Chaio Tung university, Hsinchu, Taiwan, ROC, 2001.